symmetry

MDPI

Article

On the Mechanism Controlling the Relative Orientation of Graphene Bi-Layers

Andrei Hernandez-Robles [1], David Romeu [2] and Arturo Ponce [1,3,*]

[1] Department of Physics and Astronomy, University of Texas at San Antonio, One UTSA Circle, San Antonio, TX 78249, USA; andrei.hernadezrobles@utsa.edu
[2] Instituto de Física, Universidad Nacional Autónoma de México, Apartado Postal 20-364, Mexico City 01000, Mexico; romeu@fisica.unam.mx
[3] Instituto Nacional de Astrofísica, Óptica y Electrónica, Puebla 72840, Mexico
* Correspondence: arturo.ponce@utsa.edu

Abstract: We have measured the relative orientation of rotated graphene bi-layers (RGBs) deposited by chemical vapor deposition and found that there are spontaneously occurring preferred orientations. Measurements were performed using selected area electron diffraction patterns on various regions of the RGBs. These orientations minimize the complexity of the lattice defined by the set of all possible Burgers vectors. By using a precise definition of singularity, we have been able to show that all non-singular preferred orientations are special in the sense that their angular distance $\Delta\theta$ to the closest singular orientation also complies with the definition of singularity. Our results show that these special interfaces, named secondary singular interfaces,have simpler displacement fields compared to other non-singular RGBs, implying that interfacial dislocations have fewer Burgers vectors to choose from. Since all observed orientations were found to be either singular or secondary singular, we found evidence that RGBs starting out with rotation angles far from singular orientations re-orient themselves into a nearby secondary singular state in order to simplify their strain fields. Secondary singular orientations also account for the spontaneous formation of high Σ interfaces, although the lack of a precise definition of singularity caused them to remain unnoticed.

Keywords: crystallography of interfaces; electron diffraction; coincidence site lattice; dichromatic patterns

Citation: Hernandez-Robles, A.; Romeu, D.; Ponce, A. On the Mechanism Controlling the Relative Orientation of Graphene Bi-Layers. *Symmetry* **2022**, *14*, 719. https://doi.org/10.3390/sym14040719

Academic Editor: Holger Klein

Received: 14 March 2022
Accepted: 26 March 2022
Published: 2 April 2022

1. Introduction

Two-dimensional crystals, such as graphene and metal dichalcogenides (MX_2), have risen in the interest of the scientific community due to their novel technological applications. Physical properties of confined 2D crystals can also be controlled as a function of the number of their assembled monolayers, e.g., a bilayer graphene is a tunable bandgap and its charge carrier mobility can be controlled as well [1]. The MoS_2 monolayer is a direct band-gap semiconductor, unlike its bulk nature at 1.2 eV [2,3], and, as a consequence, a remarkable increase in luminescence is experimentally measured [4]. In contrast with the extended studies of graphene 2D sheets, metal dichalcogenides exhibit a band gap shift from indirect to direct as a function of the number of S-Mo-S slabs (N), and increasing the band gap from the bulk value up to 0.6 eV for a single MoS_2 layer [2,5].Those crystals with few layers can be stacked up directly, one on top of another, with no rotation; however, properties such as those mentioned above are affected, depending on the rotation angles [6].In this way, interfacial phenomena and the analysis of the preferred orientations of the 2D-bilayer crystals are fundamental topics for their technological applications. Given that the electronic properties of rotated graphene bi-layers, hereafter referred to as rotational graphene bi-layers (RGBs), depend on the rotation angle, in this work we inquire about the possibility that there exist special orientations with low interfacial energies indicative of possible special structural and electronic properties. These rotation angles between

bi-layers are, nowadays, referred as magic angles and are responsible to unusual insulating and superconductivity properties for lower twisting angles in graphene [7,8]. Recently, a complementary continuum model has been reported, where the Fermi velocities of the moiré Dirac points not only vanish, but the bands become entirely flat at a set of punctual magic angles found at a periodicity of $\Delta\alpha \simeq 3/2$ [9].

In crystalline materials, short period interfaces identified by a small index number Σ (the ratio of the volume of the unit cell of the coincidence site lattice CSL [10] to that of the unit cell of the parent crystals) are known to be preferred, since the now classical experiments of Chaudhari and Matthews [11], who observed that small Σ interfaces occur preferentially in bi-crystals spontaneously formed during the condensation of MgO and CdO smoke. They also observed, however, that a number of bi-crystals with rotation angles lead to large values of Σ. The reason why these angles have preferred orientations has no generally accepted explanation to date.

In this work, we measured the relative orientation of spontaneously occurring RGBs in order to determine whether preferred orientations exist, and if so, we attempt to determine the factors that make them special in the hopes of obtaining useful information about their structure and related electronic properties.

Our results show that there are indeed preferred orientations with both small and large values of Σ, which, in agreement with the decades-old results of Chaudhari and Matthews, imply that the period of the interface is not a determining factor in them being preferred. Instead, special RGB orientations were characterized by a sharp decrease in the Shannon entropy [12] of their displacement spaces, implying a reduction in the number of possible Burgers vectors of interfacial dislocations.

2. Materials and Methods

Observations were made on a total of 58 RGBs obtained by chemical vapor deposition (CVD), as described in reference [13], exhibiting large areas of analyses. Rotation angles were measured directly from selected area electron diffraction (SAED) patterns obtained from individual RGBs and verified in high resolution transmission electron microscopy (HRTEM) using a transmission electron microscope, FEI-Titan, operated at 80 kV, to reduce the radiation damage to the samples.

3. Results

Figure 1a shows a typical SAED pattern and Figure 1b shows a high-resolution TEM image of two bi-layers with a 12.5° rotation angle. The distribution of rotation angles was found to be spread over the whole angular range of 0°–30°. Note that only this range needs to be considered, since the rotation angle θ and its complement $\theta_c = 60^\circ - \theta$ yield identical interfaces, except for a trivial 30° rigid body rotation. The results are summarized in Table 1 and the histogram shown in Figure 2. Additionally, we have measured the rotation angles in HRTEM images using the fast Fourier transform (FFT) in various images, as in the example shown in Figure 1b. In the table, the columns labeled θ and ξ, respectively, contain the angles measured as indicated in Figure 1 and a rational approximant ξ obtained from Equation (1). Since there are an infinite number of approximants for any given experimental accuracy, the ones given in Table 1 were calculated using continued fractions of increasingly higher orders until the difference $\Delta\theta$ (shown in the third column) between measured angles and those resulting from substituting the calculated approximant in Equation (1) was smaller than 0.05°. When the angular distance between two or more measured angles was smaller than the experimental error (0.3°), they were grouped together; in such cases, the value of θ that is given is the group's average.

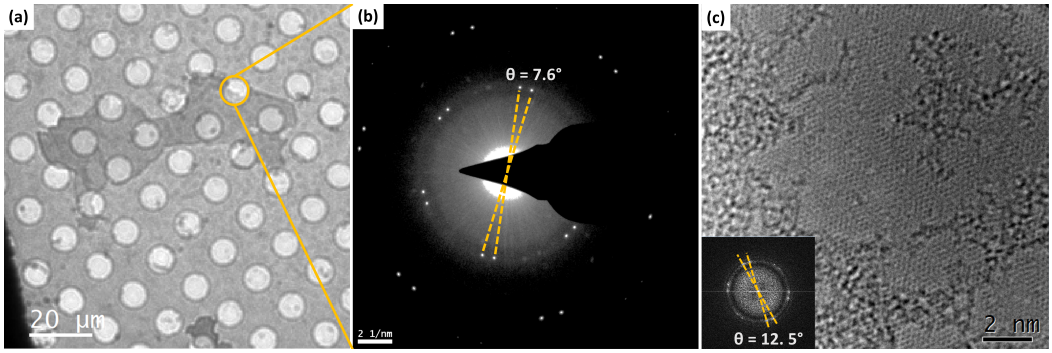

Figure 1. (**a**) Bright field image of the graphene sheets used to collect the SAED pattern. (**b**) SAED pattern of a bi-layer rotated by 7.6°. (**c**) High-resolution TEM image of two layers rotated 12.5°.

Table 1. List of measured rotation angles. The column labelled θ contains the measured angles in degrees. The column ξ contains the parameterized angles obtained from Equation (1) using continued fractions of increasingly higher orders until the difference $\Delta\theta$, shown in the third column between the rationally approximated angle and the measured one, was smaller than 0.05^o. An extra significant digit is given to the angles resulting from the average of two or more measurements.

$\theta(^\circ)$	ξ	$\Delta\theta$	$\theta(^\circ)$	ξ	$\Delta\theta$
5.70	33	0.03	18.30	$11-1/4$	0.01
6.80	29	0.04	19.03	$10+1/3$	0.00
7.60	$26+1/13$	0.00	19.70	10	0.00
9.70	$20+1/2$	0.04	20.00	$9-1/5$	0.05
10.23	$19+1/3$	0.01	20.60	$9+1/2$	0.03
10.63	$18-1/3$	0.03	21.50	$9+1/8$	0.00
11.50	$17+1/4$	0.03	22.80	$8-2/5$	0.03
12.53	$15-1/5$	0.01	23.50	$8+1/3$	0.02
13.40	$15-1/4$	0.01	23.90	$8+1/5$	0.05
14.15	14	0.04	24.50	$7-1/44$	0.02
14.90	$13+1/4$	0.00	24.80	$8-1/8$	0.01
16.03	$12+1/5$	0.05	26.80	$7+1/4$	0.04
16.50	$11-1/18$	0.00	27.70	$7+1/39$	0.02
17.20	$11+4/9$	0.01	30.00	$7-6/13$	0.01
17.80	$11+1/16$	0.00			

Figure 2 also shows the plot of the Shannon entropy [12] against θ of the displacement space, which is the space of all the possible Burgers vectors of interfacial dislocations [14]. The details of this calculation are given in the next section. For now, note that the entropy plot has sharp troughs at certain discrete values of θ, which are best described in terms of the parameterized rotation angle ξ, defined by

$$\theta = 2\tan^{-1}\frac{\sqrt{3}}{\xi} \tag{1}$$

Writing ξ as

$$\xi = x + \frac{k}{n} \tag{2}$$

With x; k and n integers, it becomes clear that entropy troughs are located at angles where k is either 1 or 0, as indicated by the value of ξ written below the most prominent troughs.

Note that all measured orientations closely match a sharp trough of the entropy curve where k is either 1 or 0. Even the angles $\theta = 17.2^\circ, 22.8^\circ$ for which $k \neq 0.1$, have decimal parts k/n very close to $1/2$; we have chosen not to make this approximation, however, in order to preserve the rule of keeping the difference between measured and rationally approximated angles smaller than 0.05°. The other value with $k \neq 1$ at 30° is a secondary

singular value, as explained below.The entropy plot was calculated with a an accuracy of 0.01°, which is an order of magnitude higher than the experimental error.

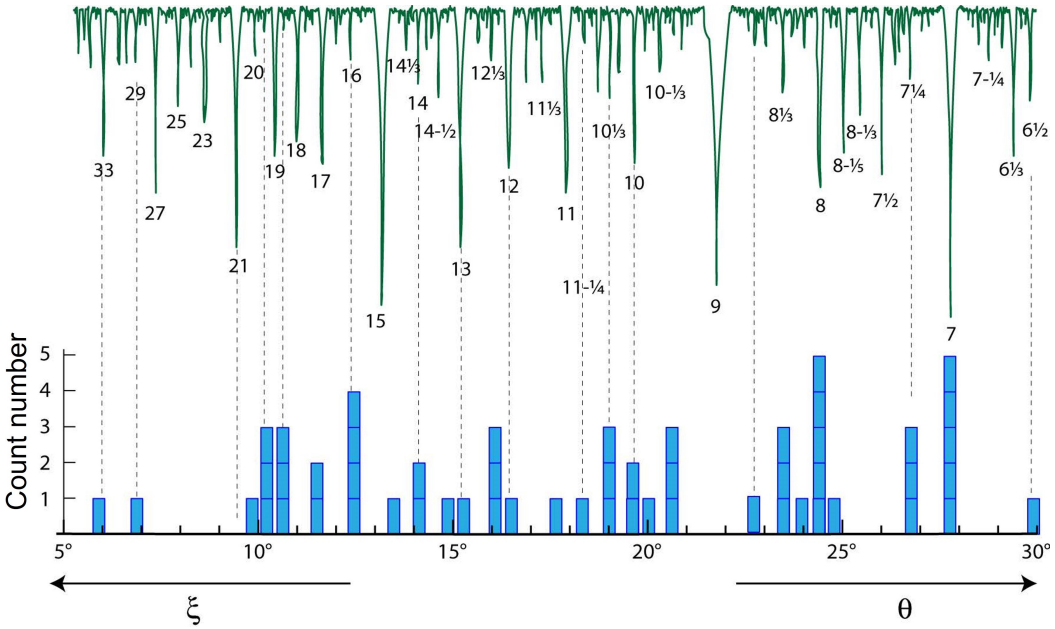

Figure 2. Bottom: Histogram of observed rotation angles between graphene sheets. The angular width of the bars is about 0.3° which is the estimated experimental error. Top: Plot of the Shannon entropy of the displacement (Burgers vector) space showing sharp troughs when $\xi = m$ or $m + 1/n$.

These results are also relatively close to the magic angles $> 5°$ reported by Tarnopolsky et. al., where their twisting angles followed a quasi-periodicity at $\Delta\alpha \simeq 3/2$ [9]. in our case, these matching angles presented sharp troughs in Figure 2, and also approximated the same periodicity. While most of the matching angles are reported in Table 1, the angle $\theta \sim 8.3°$ is included in the Shannon entropy calculation displayed in Figure 2. These angles are listed in Table 2.

Table 2. List of measured rotation angles and magic angles 5–11.5°.

	Matching Angles				
θ	5.7	6.8	8.3	9.7	11.5
α [9]	5.276	6.795	8.313	9.829	11.345

The physical explanation of these results can be simply stated in terms of the lattice type formed by the vectors of the displacement field of each interface, as discussed in the following subsections.

3.1. Primary and Secondary Singular States

According to Bollmann [14], there are special low energy interfaces he called "preferred states" which contain only primary dislocations, i.e., dislocations with Burgers vectors belonging to the crystal (graphene) lattices that compose the interface. Since Bollmann did not have a formal definition of a preferred state, he made the usual vague assumption that they were coincidence orientations with an unspecified small value of Σ. Bollmann further assumed that under small angular deviations, $\Delta\theta$ form a preferred state, and the interface would try to preserve its low energy configuration by concentrating the strain field in what he called secondary dislocations.In contrast with the primary ones, secondary dislocations have smaller non crystalline Burgers vectors belonging to the DSC lattice, which is the lattice formed by a set of vectors joining the sites of the composing lattices. Bollmann showed that secondary Burgers vectors could be calculated from a different interface formed by the DSC

lattice, and a copy of itself rotated by $\Delta\theta$. We shall refer to this interface, which is central to the results of this work, as the "secondary interface" or "secondary state". The experimental observation of secondary dislocations [15], with dislocation spacings in accordance with Bollmann's hypotheses, confirmed the physical significance of the secondary interface. Preferred states will hereafter be referred to as singular states or singular interfaces to follow the more common usage [10].

It has been shown [16] that the rotation angles θ_x resulting from the substitution of an integer x for the rational parameter ξ in Equation (1) give rise to singular interfaces containing only primary dislocations. It is interesting to note that the set of integers actually partitions the angular space into equivalence classes $x - 1/2 \leqslant \xi < x + 1/2$ whose normal mode is the singular interface at θ_x [17].

In view of the above, any RGB with rotation angle $\theta = \theta_x + \Delta\theta$ can be thought of as having two components or states: a singular primary state with rotation angle θ_x and a secondary state with rotation angle $\Delta\theta$. It now makes sense to inquire under what circumstances the secondary state is, itself, singular.

To do this, we use Equation (1) to parameterize θ_x and $\Delta\theta$ as

$$\tan\frac{\theta_x}{2} = \frac{\sqrt{3}}{x}; \quad \tan\frac{\Delta\theta}{2} = \frac{\sqrt{3}}{\zeta} \tag{3}$$

for some of the integer x and rational ζ. After some trigonometry, we find that $\zeta = (3 + \xi x)/(x - \xi)$, and in substituting $x + \delta$ for ξ, we find that $-\zeta = x + \frac{T}{\delta}(3 + x^2)$, which shows that secondary states are, themselves, singular (integer ζ) when $\delta = 1/n$ or $\delta = (3 + x^2)/n$, i.e., when $k = 1$ in Equation (2) or $(3 + x^2)/n$ is an integer. This is the case of $\theta = 30^\circ$, since (see Table 1) $(3 + 7^2)/13$ is an integer. Therefore, we conclude that the minima in the entropy plot of Figure 2 correspond to RGBs which are either singular states or non-singular ones with a singular secondary component. In the next section, we describe the structural implications of this result.

3.2. The Displacement Space lattice

The formal framework for calculating the structure of the displacement space has been given elsewhere [16]. For completeness, we provide a simpler geometrical description here. Figure 3 shows, on the left, the dichromatic complex of a graphene bi-layer, and on the right, the set of (encircled) vectors join the displacement vectors, whose size is smaller than half a lattice vector of the graphene lattice. The displacement vectors that fulfill this condition are vectors of the DSC lattice that fall within a window given by the cut-projection formalism [16] (see Figure 4), and the circles around each vector are the locus of points of high strain and high electronic density in the interfacial plane between the graphene layers. This pattern not only provides a simpler crystallographic description of the interface by turning the dichromatic complex into a monochromatic one, but, more importantly, it establishes a mapping between the configuration and displacement spaces. Every vector in the displacement space is linked to all the sites of the monochromatic pattern that encircle the dichromatic points separated by that vector.

If ξ is a rational number, which it always is given the experimental error, then both the set of displacement vectors and its associated monochromatic pattern form a lattice whose degree of complexity depends on ξ. The complexity of the displacement space lattice (DSL) (multiplied by one inside the window and zero outside) is what the Shannon entropy calculation, shown in Figure 2, measures. Figure 4 shows examples of DSLs of varying complexities.

The entropy plot in Figure 2 was calculated by evaluating every 0.01° of the Shannon entropy of the distribution of bond lengths in the range [0.0–0.2] in lattice spacing units, divided into 30 intervals. Varying this range and/or the number of intervals may produce slight changes in the relative depths of the troughs, but there is always a sharp local entropy minimum when ξ is an integer (singular states) or when its decimal part is the inverse of an integer (secondary singular states).

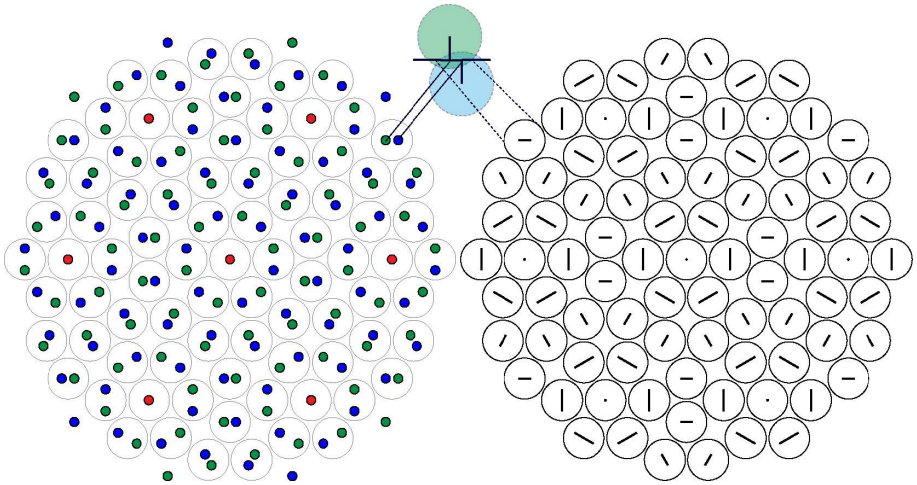

Figure 3. Left: dichromatic complex of the singular interface $\xi = 7, \Sigma = 13$ with green and blue circles representing the sites of each graphene sheet, as indicated in the central diagram illustrating the disposition of carbon atoms on either side of the interfacial plane. Red circles are coincidence sites. **Right**: Graphical representation of the displacement field as lines joining the sites, whose distance is smaller than half a lattice vector (one atomic radius). The circles around the midpoints of the displacement vectors simplify the crystallographic description of the interface by turning the dichromatic complex into a monochromatic one, whose sites are points of high strain where electron clouds overlap.

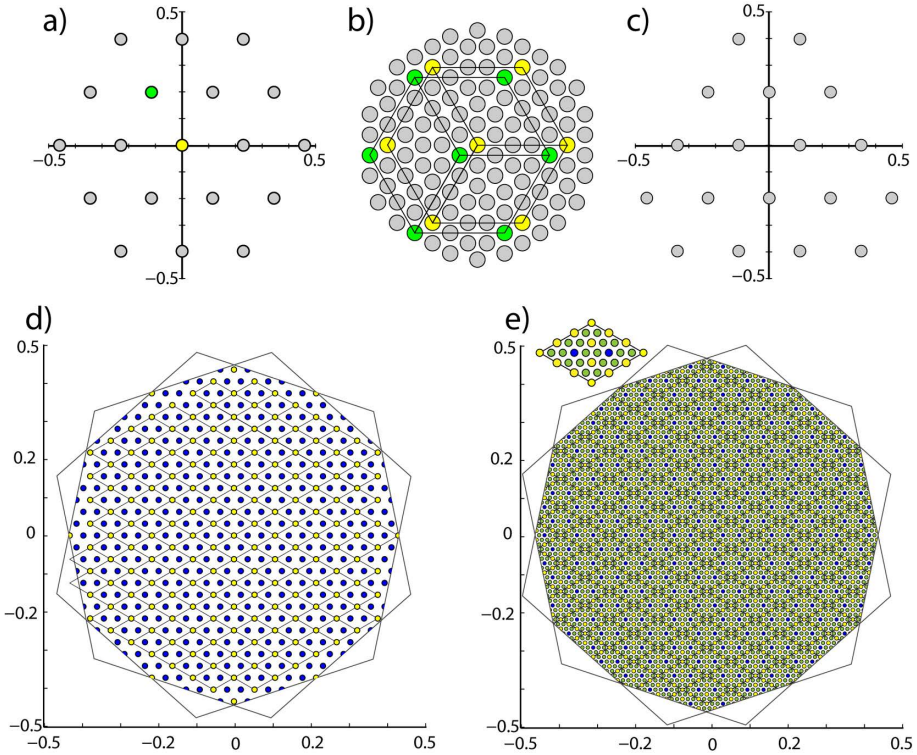

Figure 4. (**a**) Primitive DSL of the singular interface $\xi = 15, \Sigma = 19$ with both graphene sheets sharing a common origin. (**b**) Monochromatic pattern associated to DSL at left with green and yellow circles identifying sites with the displacements marked with the same colors in (**a**). (**c**) same DSL as (**a**) but with graphene sheets relatively displaced by the vector (0.12; 0.12) illustrating that relative sheet displacements only shift the DSL without altering its structure. (**d**,**e**) Non singular DSLs with primary states $\Sigma_{x=5} = 7$. (**d**) $\xi = 5 + \frac{1}{5}, \Sigma = 751$; (**e**) $\xi = 5 + \frac{3}{13}, \Sigma = 1591$ with an amplified unit cell at the top to make its contents clearer. The rotated hexagons identify the window used in the cut-projection formalism 14 used to calculate the DSLs.

4. Discussion

Given the hexagonal symmetry of the dichromatic pattern, each DSL point is associated with a subset of monochromatic sites that form a primitive hexagonal lattice (see Figure 4). An example of this is the hexagonal sublattice of coincidence sites associated with the DSL origin.

The DSL is always a simple primitive lattice when its unit cell is built using the basis vectors of the DSC lattice [18]. However, its degree of complexity is best described in terms of the subset of DSL points associated with hexagonal lattices, whose unit cells have the same areas as the unit cell of the CSL of the singular primary state; the physical significance of this unit cell is that its points represent Burgers vectors of primary dislocations. Using this unit cell, all primary states have a low entropy of the primitive DSL. The higher the order of the continued fraction expansion of ξ, the higher the contents of the unit cell. Figure 4 illustrates three levels of complexity of the displacement space. We conclude that crystallographic distinctions between DSLs, and their effects on the number of points that fit inside the window, accounts for the sharp entropy minima of singular and secondary singular interfaces.

In order to conclusively confirm that secondary singular interfaces are preferred states, ab-initio calculations need be performed in the vicinity of secondary singular interfaces at angular intervals close to the value of 0.01° used in the entropy calculation. This would entail calculations with much larger periodicities than the ones usually performed. We believe that the high computing cost of such calculations, coupled with the lack of a precise definition of singularity, have caused secondary singular interfaces to remain unnoticed.

In the meantime, although the Shannon entropy is not a measure of energy, it can be argued that since the latter depends on the distribution of interatomic distances, it is possible that interfaces with simpler distributions have lower energies. This is, after all, the role that dislocations play in reducing the elastic energy of crystalline materials.

Considering singular secondary interfaces as preferred (local energy minima) orientations not only accounts for the results obtained here for graphene, but it also explains other observations of spontaneously occurring nonsingular interfaces. For example, in the case of 001 twist interfaces in the cubic system, there are no singular orientations in the interval 36.875°, ($\xi = 3$) to 53.13°, ($\xi = 2$), both $\Sigma = 5$ interfaces. Yet, a number of interfaces in this range were observed by Chaudhari and Matthews [11]; in particular, those seen in their histogram near 39°; 41° and 42°, which appear to be the secondary singular $\xi = 3 - \frac{1}{6}(\theta = 38.88^\circ, \Sigma = 325)$, $\xi = 3 - \frac{1}{3}(\theta = 41.11^\circ, \Sigma = 73)$ and $\xi = 3 - \frac{1}{2}(\theta = 43.61^\circ, \Sigma = 29)$. Although under the vague small Σ criterion, $\Sigma 29$ could have been considered a preferred state by Bollmann. The fact is that its DSL is not primitive, evidencing that a small value of Σ does not imply singularity.

5. Conclusions

Numerous calculations [10] have shown that singular interfaces have lower energies. This, however, does not answer the question of what happens with RGBs that start out far away from a singular orientation and do not have enough kinetic energy to rotate into a singular state. For example, Figure 2 shows that there are no singular RGBs between $\xi = 7(\theta = 27.8^\circ, \Sigma = 13)$, and $\xi = 8(\theta = 24.4^\circ, \Sigma = 67)$ so that any bi-layer starting to grow in the middle of this 3.4° interval would have to rotate more than one degree to find a singular orientation. Our results suggest that bi-layers starting out with a random rotation angle will try to rotate into a nearby secondary singular state. This appears to have been the case with the three $\Sigma = 889$ bi-layers observed at $\theta = 26.8^\circ$.

The 0.3° experimental accuracy provided by the present experimental setup is not enough to experimentally confirm that secondary singular states are indeed the preferred low energy states; to do this, an experimental accuracy equal to, or better than, the 0.01° step used in the entropy calculation would be required. In spite of this, the consistent observation of RGBs near entropy minima, and the fact that secondary singular interfaces have been observed in other systems, supports this hypothesis.

Given the relevance of determining the mechanisms that control the precise orientation in designing materials with tailor-made properties, our results evidence the need to perform ab-initio calculations at, and close to, secondary singular orientations. Moreover, experiments using more accurate techniques to measure rotation angles are also needed to clarify this important point.

Author Contributions: Conceptualization and geometrical models, D.R.; Editing, electron microscopy analysis and measurements, A.P and A.H.-R.; Supervision A.P. All authors have read and agreed to the published version of the manuscript.

Funding: The authors thank the technical support in the use of the transmission electron microscope at CIQA. This work was supported by CONACYT FOMIX PUE-2018-03-02-84557 and A1-S-35309.

Institutional Review Board Statement: Not applicable.

Informed Consent Statement: Not applicable.

Data Availability Statement: Not applicable.

Acknowledgments: The authors wish to acknowledge the groups who provided the graphene samples: Jing Kong from the RLE-Nanomaterials and Electronics group at Massachusetts Institute of Technology MIT. A.H.R thanks to ConTex Doctoral Fellowship program #2019-000027-01EXTF-00125.

Conflicts of Interest: The authors declare no conflict of interest.

References

1. Zhang, Y.; Tang, T.T.; Girit, C.; Hao, Z.; Martin, M.C.; Zettl, A.; Crommie, M.F.; Shen, Y.R.; Wang, F. Direct observation of a widely tunable bandgap in bilayer graphene. *Nature* **2009**, *459*, 820–823. [CrossRef] [PubMed]
2. Radisavljevic, B.; Radenovic, A.; Brivio, J.; Giacometti, V.; Kis, A. Single-layer MoS2 transistors. *Nat. Nanotechnol.* **2011**, *6*, 147–150. [CrossRef] [PubMed]
3. Kam, K.K.; Parkinson, B.A. ChemInform Abstract: Detailed photocurrent spectroscopy of the semiconducting group vib transition metal dichalcogenides. *Chem. Inf.* **1982**, *13*, 463–467. [CrossRef]
4. Eda, G.; Yamaguchi, H.; Voiry, D.; Fujita, T.; Chen, M.; Chhowalla, M. Correction to Photoluminescence from Chemically Exfoliated MoS 2. *Nano Lett.* **2012**, *12*, 5111–5116. [CrossRef]
5. Mak, K.F.; Lee, C.; Hone, J.; Shan, J.; Heinz, T.F. Atomically thin MoS2: A new direct-gap semiconductor. *Phys. Rev. Lett.* **2010**, *105*, 136805–136809. [CrossRef]
6. De Trambly Laissardière, G.; Mayou, D.; Magaud, L. Localization of dirac electrons in rotated graphene bilayers. *Nano Lett.* **2010**, *10*, 804–808. [CrossRef] [PubMed]
7. Cao, Y.; Fatemi, V.; Demir, A.; Fang, S.; Tomarken, S.L.; Luo, J.Y.; Sanchez-Yamagishi, J.D.; Watanabe, K.; Taniguchi, T.; Kaxiras, E.; et al. Correlated insulator behaviour at half-filling in magic-angle graphene superlattices. *Nature* **2018**, *556*, 80–84. [CrossRef] [PubMed]
8. Cao, Y.; Fatemi, V.; Fang, S.; Watanabe, K.; Taniguchi, T.; Kaxiras, E.; Jarillo-Herrero, P. Unconventional superconductivity in magic-angle graphene superlattices. *Nature* **2018**, *556*, 43–50. [CrossRef] [PubMed]
9. Tarnopolsky, G.; Kruchkov, A.J.; Vishwanath, A. Origin of Magic Angles in Twisted Bilayer Graphene. *Phys. Rev. Lett.* **2019**, *122*, 106405. [CrossRef]
10. Priester, L. From Theory to Engineering; In *Grain Boundaries*; Springer: Dordrecht, The Netherlands, 2013; Volume 172.
11. Chaudhari, P.; Matthews, J.W. Coincidence twist boundaries between crystalline smoke particles. *J. Appl. Phys.* **1971**, *42*, 3063–3066. [CrossRef]
12. Shannon, C.E. A Mathematical Theory of Communication. *Bell Syst. Tech. J.* **1948**, *27*, 379–423. [CrossRef]
13. Reina, A.; Jia, X.; Ho, J.; Nezich, D.; Son, H.; Bulovic, V.; Dresselhaus, M.S.; Jing, K. Large area, few-layer graphene films on arbitrary substrates by chemical vapor deposition. *Nano Lett.* **2009**, *9*, 30–35. [CrossRef] [PubMed]
14. Bollmann, W. *Crystal Defects and Crystalline Interfaces*; Springer: Berlin/Heidelberg, Germany, 1970. [CrossRef]
15. Sun, C.P.; Balluffi, R.W. Secondary grain boundary dislocations in [001] twist boundaries in MgO I. Intrinsic structures. *Philos. Mag. A—Phys. Condens. Matter Struct. Defects Mech. Prop.* **1982**, *46*, 49–62. [CrossRef]
16. Romeu, D. Interfaces and quasicrystals as competing crystal lattices: Towards a crystallographic theory of interfaces. *Phys. Rev. B—Condens. Matter Mater. Phys.* **2003**, *67*, 024202–024234. [CrossRef]
17. Romeu, D.; Gómez-Rodríguez, A. Recurrence properties of O-lattices and the classification of grain boundaries. *Acta Crystallogr. Sect. A Found. Crystallogr.* **2006**, *62*, 411–412. [CrossRef] [PubMed]
18. Warrington, D.H. The coincidence site lattice (csl) and grain boundary (dsc) dislocations for the hexagonal lattice. *Le J. De Phys. Colloq.* **1975**, *36*, C4-87–C4-95. [CrossRef]